

Supporting Information

**Preserved S-scheme band structure of graphitic carbon
nitride/bismuth oxobromide after the introduction of black
phosphorous driven by internal electric field: achieving significantly
enhanced photocatalytic performance**

Lijun Chen^a, Feihong Wang^a, Jiahao Zhang^a, Hongyuan Wei^{a}, Leping Dang^{a*}*

*^a Green Separation & Chemical Process Safety Lab, School of Chemical Engineering
and Technology, Tianjin University, Tianjin 300072, PR China*

Lijun Chen, lijunchen@tju.edu.cn

Feihong Wang, feihongwang@tju.edu.cn

Jiahao Zhang, zhangjh223@tju.edu.cn

** Corresponding authors*

Mail address: dangleping@tju.edu.cn (L.P. Dang), david.wei@tju.edu.cn (H.Y. Wei).

The ORCID iD of submitting author, Prof. Leping Dang: 0000-0003-1713-542

Total number of texts: 4

Total number of figures: 16

Total number of tables: 3

Text S1 Specific instructions on physicochemical characterization:

The morphologies of synthesized samples were observed using scanning electron microscopy (SEM, Regulus 8100, Hitachi, Japan), and the height of BPs was tested using an atomic force microscope (AFM, Dimension icon, Bruker, Germany). A transmission electron microscope (TEM, JEM-F200, JOEL, Japan) equipped with an energy dispersive spectrometer (EDS) was employed to characterize the microstructure and elemental distribution. The specific surface area and pore size distribution were determined by BET (ASAP2460, Micromeritics, US) at the temperature of 77 K. The crystal structures of samples were measured using an X-ray diffraction (XRD) spectrometer (D8 Advance, Bruker, Germany) irradiated with a Cu-K α target ($\lambda = 1.5406 \text{ \AA}$) at a scanning speed of 5 °/min between the range of 10°~80°. The chemical composition and valance state were analyzed by X-ray photoelectron spectroscopy (XPS, ESCALAB Xi+, ThermoFisher Scientific, UK) with Al-K α radiation. Ultraviolet/visible diffuse-reflectance spectra (UV/Vis-DRS, Lambda 750S, PerkinElmer, UK) were carried out to determine the photo-response range. Photoluminescence spectroscopy (PL) and time-resolved PL (TRPL) decay spectroscopy were measured by a fluorescence spectrometer (FLS1000, Edinburgh, UK). The electron paramagnetic resonance (EPR) was tested to confirm the reactive oxidized species (EMXplus-6/1, Bruker, Germany), where the 5, 5-dimethyl-1-pyrroline-N-oxide (DMPO) was used as a capture agent in aqueous or methanol suspension of samples to trap the $\cdot\text{OH}$ and $\cdot\text{O}_2^-$, respectively.

Text S2 Specific instructions on Photoelectrochemical characterization:

All electrochemical tests were conducted on an electrochemical workstation (CHI660E, Chenhua, China) with a standard three electrodes system, where a Pt flake, an Ag/AgCl electrode, and the prepared photoelectrode were used as a counter electrode, reference electrode, and the working electrode, respectively. The working photoelectrode was prepared on an indium-doped tin oxide (ITO) glass substrate that was cleaned by sonication in ethanol for 2 h and blow dry with N₂. 10 mg of photocatalyst powder and 50 μL Nafion solution as a binder were dispersed uniformly to 1 mL ethanol. Then 150 μL of the slurry was spread onto ITO substrate with a 1.3 cm² effective area. After air drying, the processed substrate was annealed at 220 °C for 2 h under N₂ gas protection to improve the adhesion and evaporate the residual solvents.

The photocurrent response curve (PRC) was tested in 0.5 M N₂SO₄ with a 300 W Xe lamp equipped with a 420 nm cut-off filter as a light source with a bias voltage of 0.5 V. Electrochemical impedance spectroscopy (EIS) was carried out by using the alternating current amplitude of about 0.2 V between the frequency range of 0.1 Hz-100 kHz under open circuit potential in the mixed solution of potassium ferricyanide (K₃[Fe(CN)₆]), potassium ferrocyanide (K₄Fe(CN)₆) and potassium chloride (KCl) with the same concentration of 0.1M. The Mott-Schottky (M-S) measurement was conducted to obtain the flat band potential E_{fb} ranged from -1.0 to 1.0 V (vs Ag/AgCl) for CNs and BPs, 0 to 2.0 V (vs Ag/AgCl) for BOB with a frequency of 1 kHz in 0.5 M N₂SO₄ under an amplitude of 0.01 V.

Text S3 The instruction for photocatalytic experiments.

The photocatalytic activities of as-prepared samples were evaluated by photocatalytic degradation of various pollutants under irradiation of Xe lamp (PLS-SXE300, Perfect light, China) at 300 W with an ultraviolet cutoff filter ($\lambda < 420$ nm) at a fixed temperature of 25 °C. Firstly, 50 mg of photocatalyst was added to 200 mL of pollutant solution with a concentration of 20 mg/L unless specified. Before irradiation, 30 min of ultrasonic treatment was carried out to promote the dispersion of the catalyst, followed by magnetic stirring in the dark for 30 min to ensure the adsorption/desorption equilibrium between photocatalyst powders and pollutants. At given time intervals, 4 mL of water sample was taken out by a syringe equipped with a 0.22 μ m polyethersulfone filter with good hydrophilicity to remove catalyst particles. The concentration of targeted pollutant was determined with a UV-Visible spectrophotometer at the maximum absorption wavelength, and in specific, 357 nm, 274 nm, 554 nm, 270 nm, and 224 nm for the TCH, ciprofloxacin (CIP), rhodamine b (RhB), phenol, bisphenol a (BPA), respectively. Among these pollutants, the TCH is selected as a model pollutant to investigate the photocatalytic performance of as-prepared catalysts deeply, and other pollutants are chosen to evaluate the adaptability of photocatalysts.

The removal ratio R was calculated according to the following formula:

$$R = \frac{C_0 - C}{C_0} \times 100\%$$

C_0 and C are the initial and final concentrations of the pollutants (mg/L), respectively.

The mineralization degree (MD) of the targeted pollutant was determined by the change of total organic carbon (TOC), which was tested by a Shimadzu TOC-LCSH/CPH analyzer through the wet combustion method. The MD was calculated by

the following equation.

$$MD = \frac{TOC_0 - TOC}{TOC_0} \times 100\%$$

TOC₀ and TOC refer to the total organic carbon concentration (mg/L) of water samples before and after the photocatalytic reaction, respectively.

Text S4 Determination of degradation intermediates.

The possible degradation intermediates of TCH produced during the photocatalytic reaction were identified by ultra-performance(Ultimate 3000 UHPLC-Q Exactive, Thermo Scientific, US). LC process was performed using an Eclipse Plus C18 chromatographic column (3.5 μm, 100 mm × 4.6 mm) with an injection volume of 10 μL at a flow rate of 0.4 mL/min. The operation temperature was controlled at 30 °C. The elution was performed via 0.1% (v/v) of formic acid aqueous solution (A) and acetonitrile (B). Linear gradient elution was set as follows: the initial 90% A was reduced to 10% A over 10 min and kept for another 4 min. Then the mobile phase A returned to 90% in 1 min and maintains for 1 min. MS experiments were carried out in positive electrospray ionization (ESI+) mode under the following working conditions: capillary voltage of 3.8 kV, dry heater temperature of 300 °C, nebulizer of 15 psi, dry gas (N₂) flow rate of 10 L/min, and the scan range was set from 200 to 600 m/z [1].

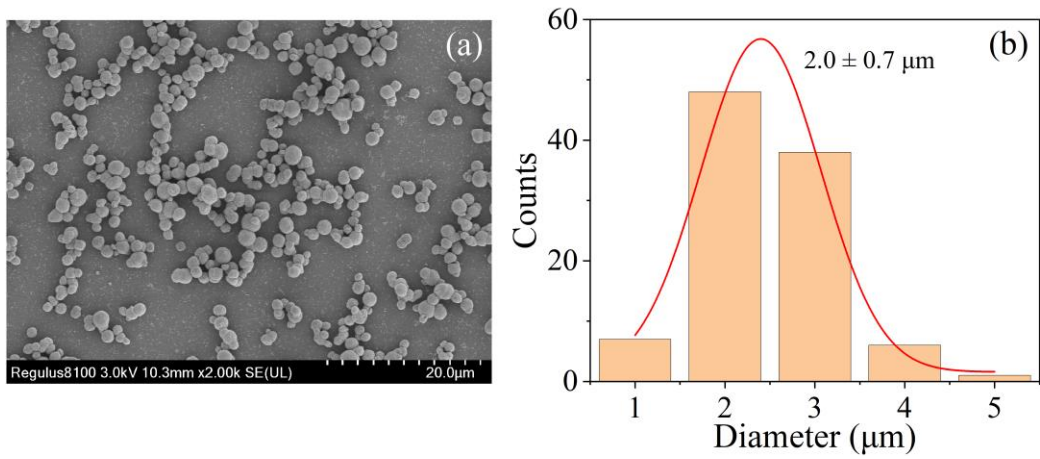


Fig. S1. The (a) SEM of BOB spheres at low resolution and (b) size distribution of BOB spheres.

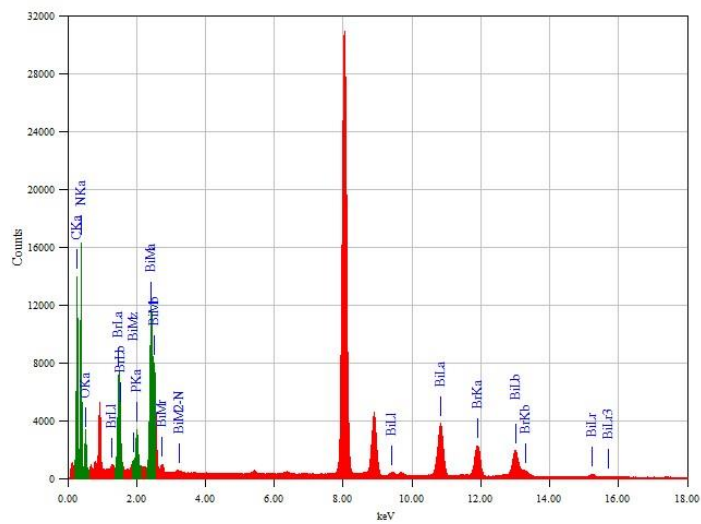


Fig. S2. The EDS result of the 3BPs/CNs/BOB.

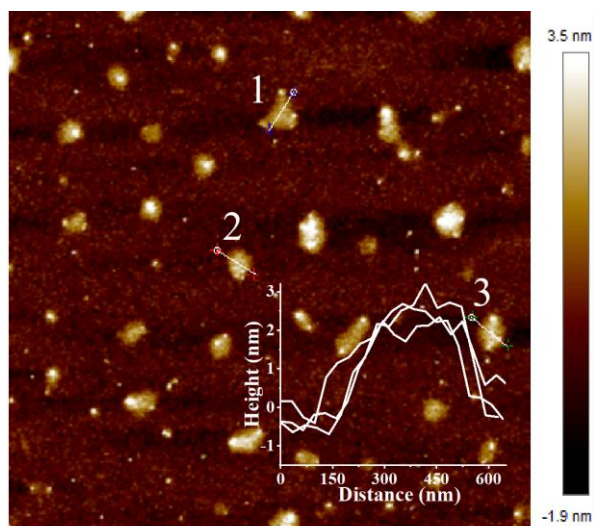


Fig. S3. The AFM of exfoliated BPs.

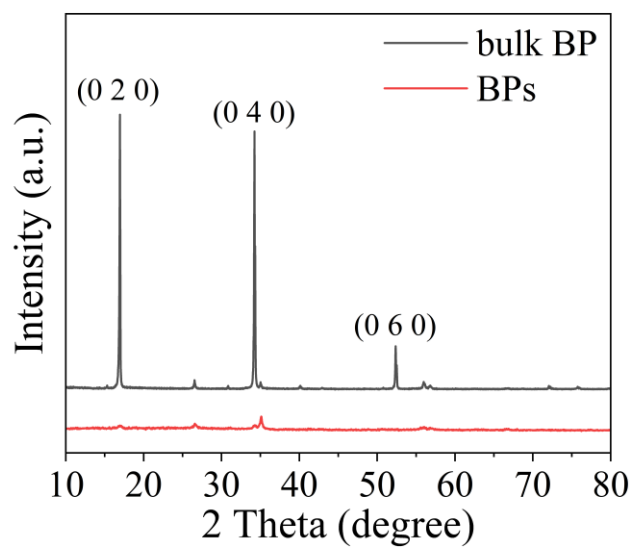


Fig. S4. The XRD pattern of bulk BP and exfoliated BPs.

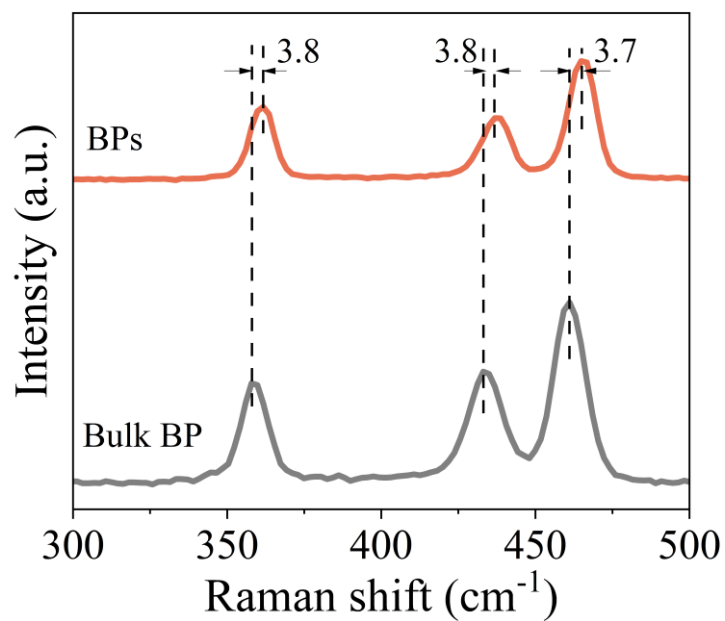


Fig. S5. The Raman spectra of bulk BP and BPs.

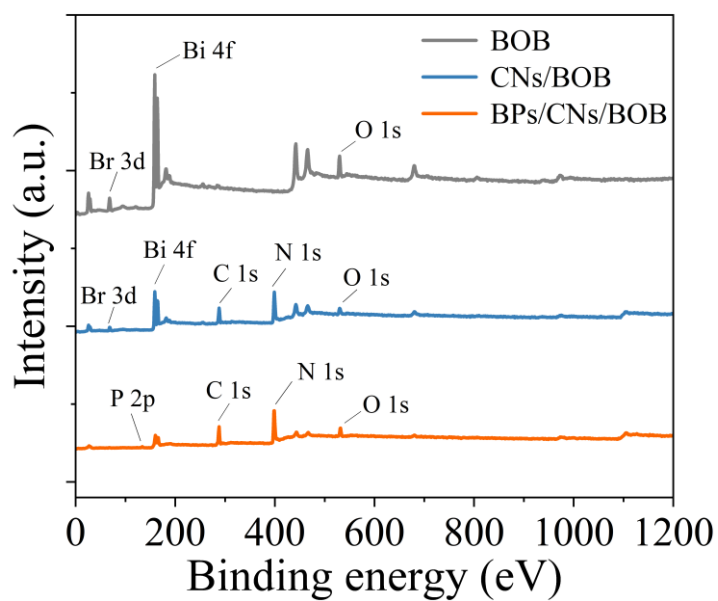


Fig. S6. The XPS full spectrum of BOB, CNs/BOB, and BPs/CNs/BOB.

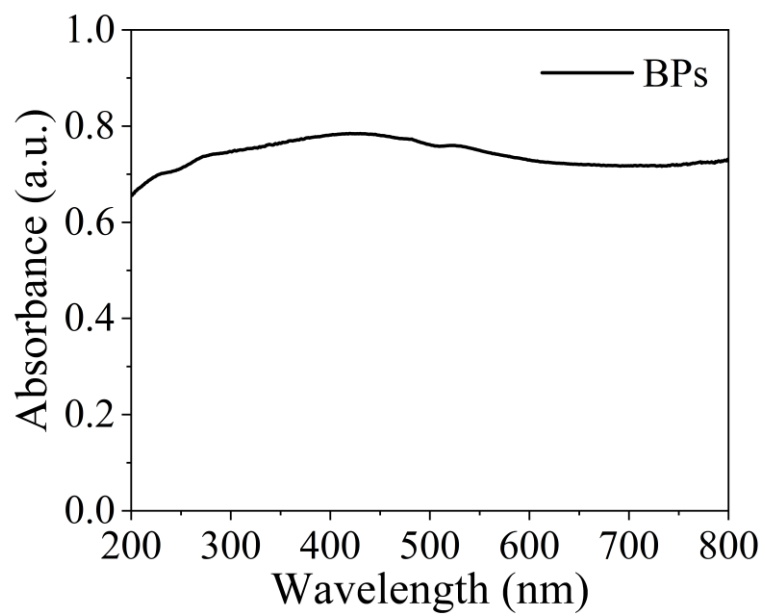


Fig. S7. The DRS spectra of BPs.

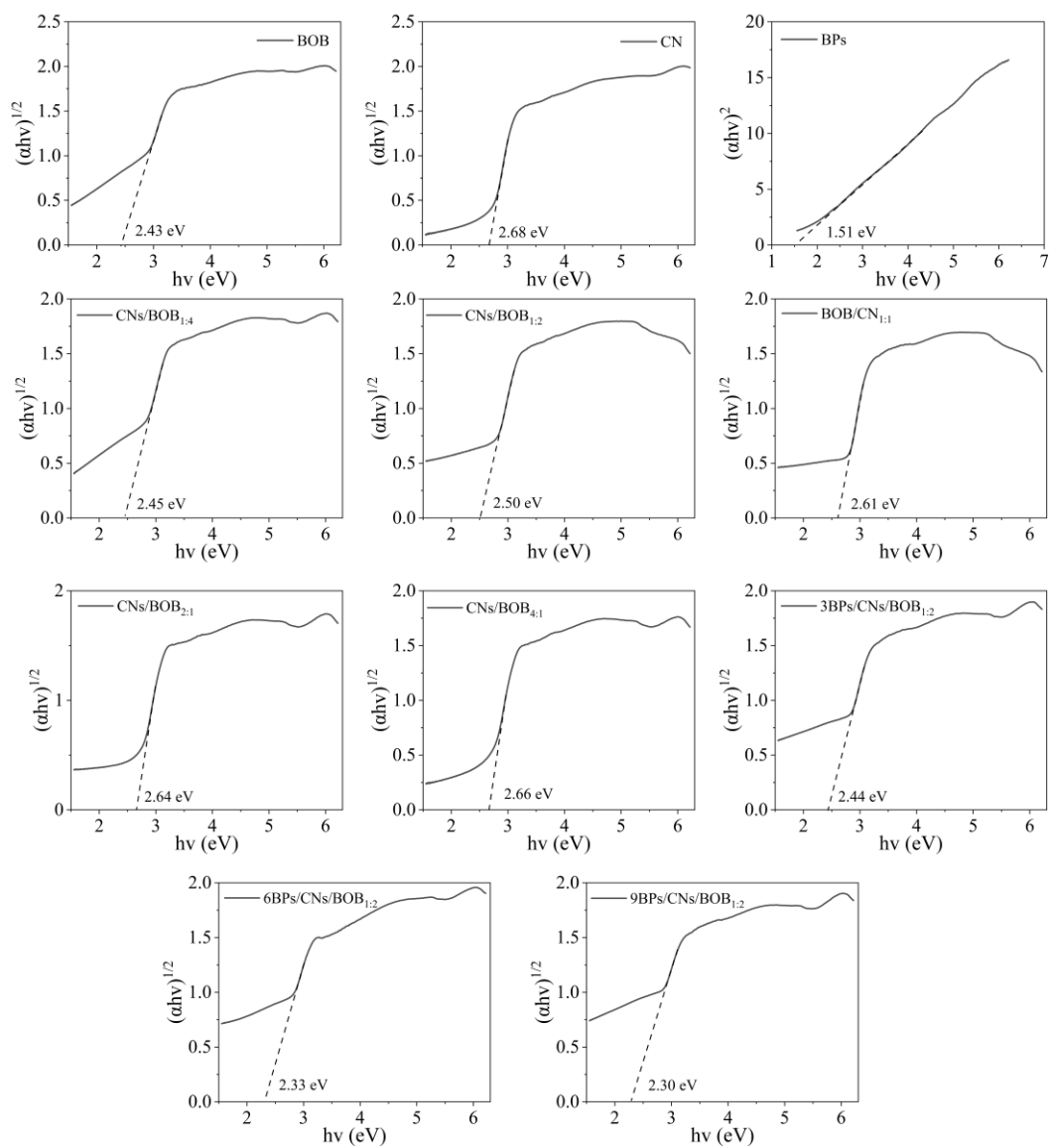


Fig. S8. The respective Tauc plots of as-prepared samples.

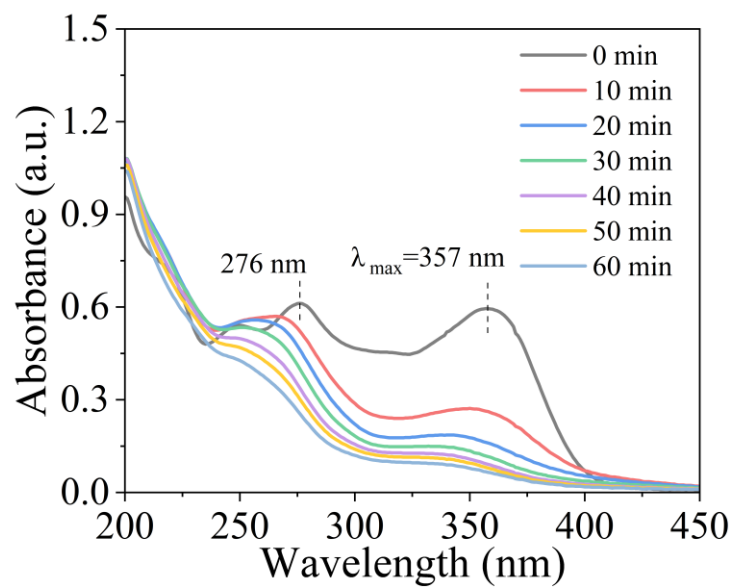


Fig. S9. The absorbance spectrum of TCH at different degradation time points.

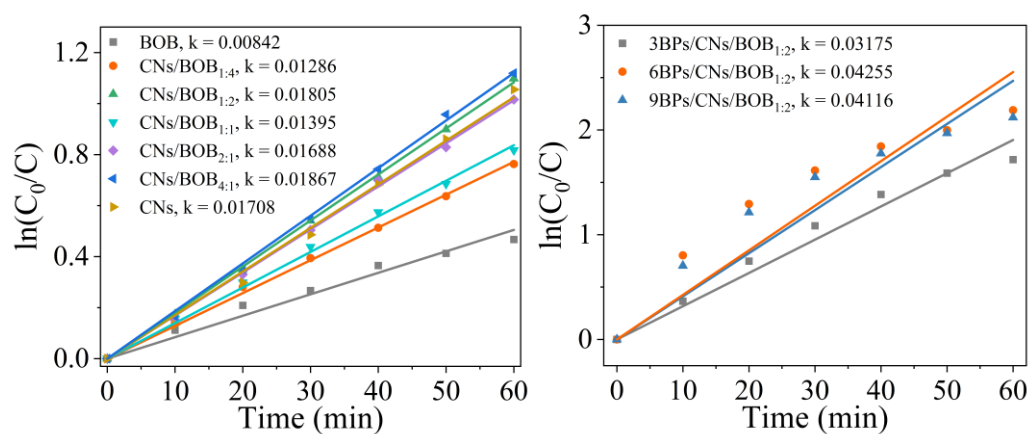


Fig. S10. The quasi-first-order kinetic curves of as-prepared samples.

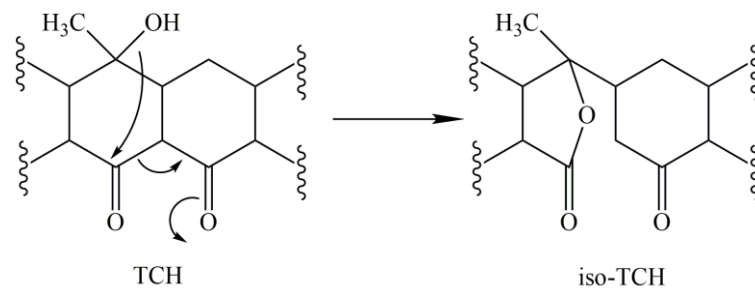


Fig. S11. The transformation process of TCH to iso-TCH with lactone structure under alkaline conditions.

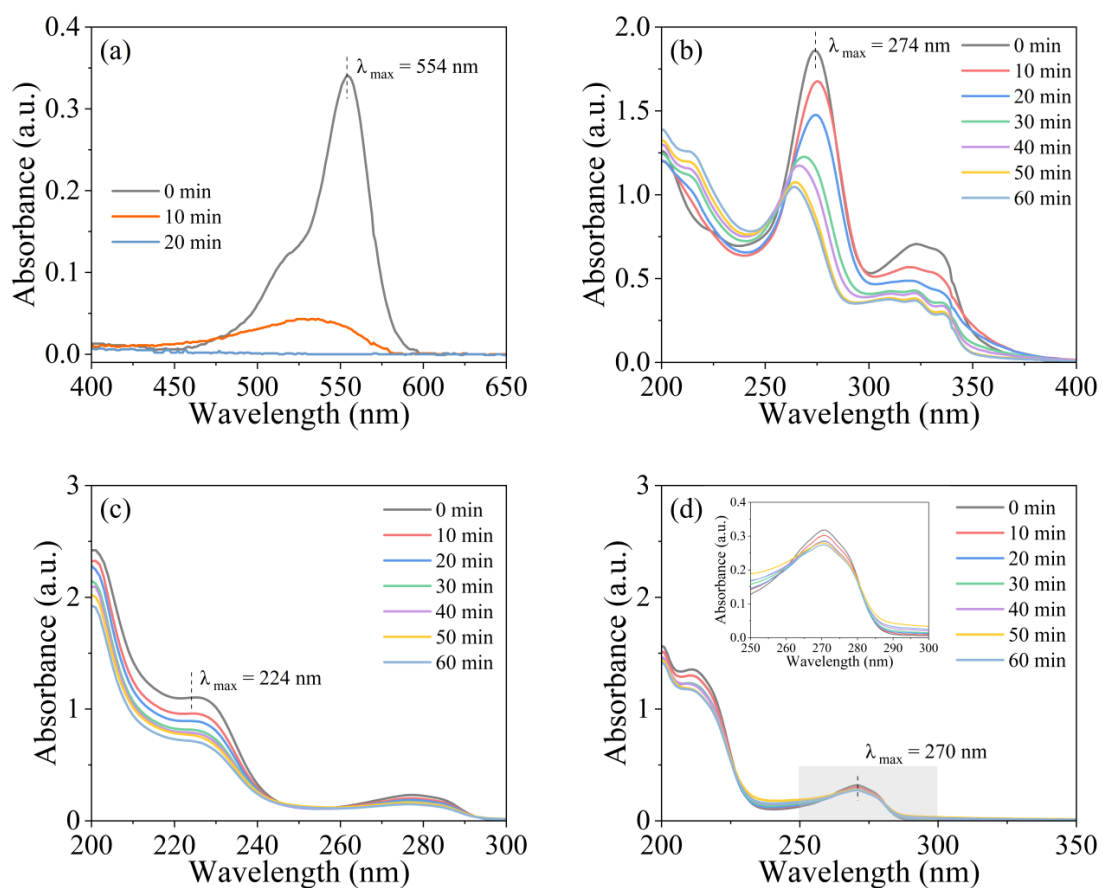


Fig. S12. The absorbance spectrum of (a) RhB, (b) CIP, (c) BPA, and (d) phenol at different degradation times.

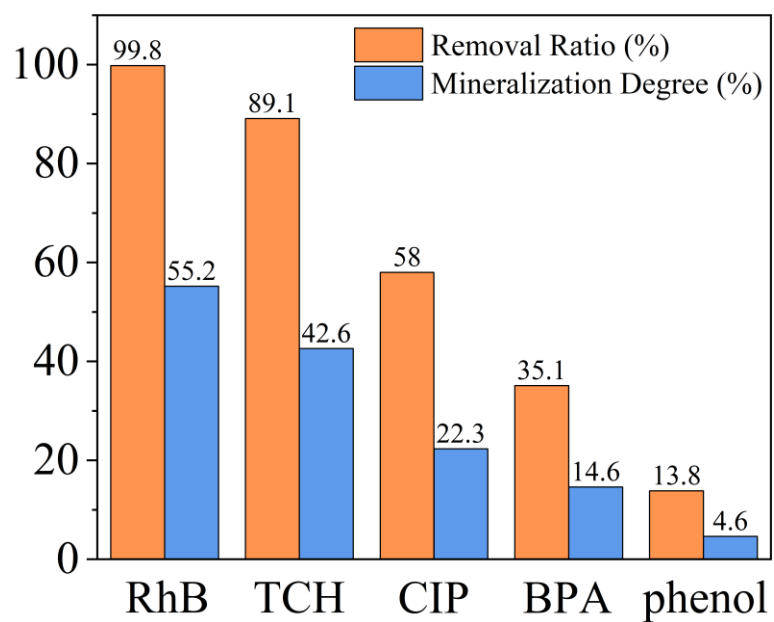


Fig. S13. The removal ratio and mineralization degree of various pollutants.

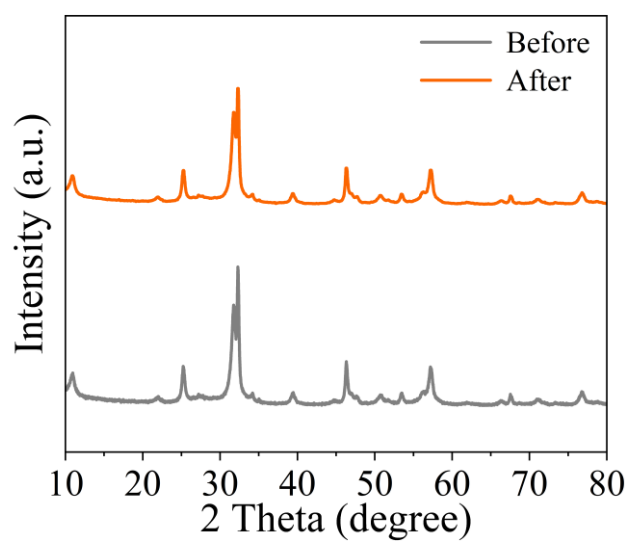


Fig. S14. The XRD pattern of 6BPs/CNs/BOB_{1:2} before and after the cyclic degradation experiments.

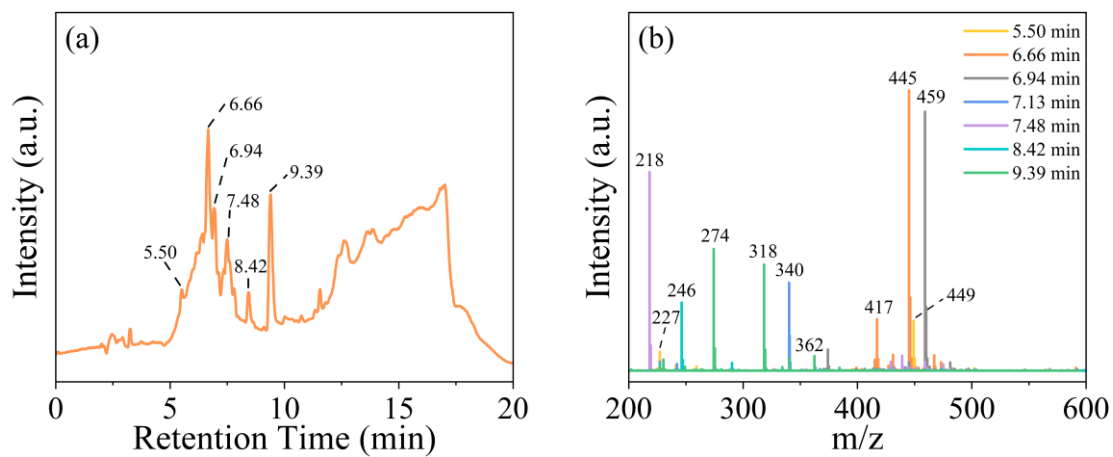


Fig. S15. The (a) total ions chromatograph and (b) MS spectra at a certain retention time with relatively higher abundance (after 60 min of degradation).

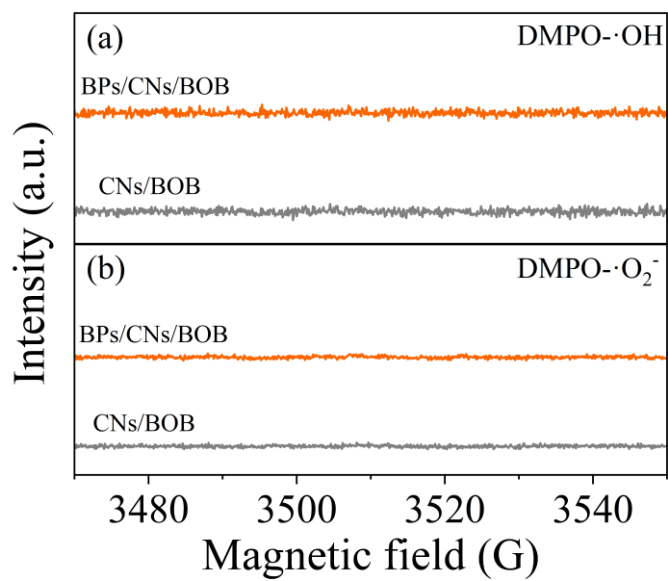


Fig. S16. The EPR test results of the (a) $\text{DMPO}\cdot\cdot\text{OH}$ and (b) $\text{DMPO}\cdot\cdot\text{O}_2^-$ in the dark.

Table S1

The mass ratio of respective elements in the composite 3BPs/CNs/BOB was obtained from the EDS result. (The mass ratio of BPs to CNs/BOB was calculated to be 2.82%/97.18% \approx 2.90%)

Sample	element	The mass ratio (%)	Total (%)
CNs	C	20.68	35.54
	N	14.86	
BOB	O	2.04	61.64
	Bi	46.31	
	Br	13.29	
BPs	P	2.82	2.82

Table S2

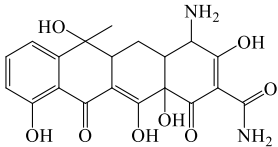
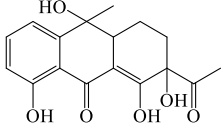
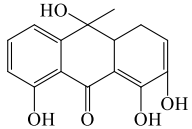
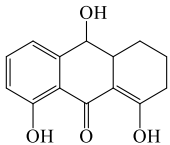
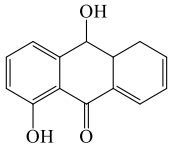
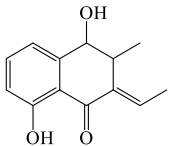
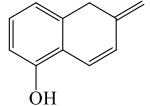
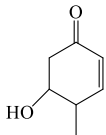
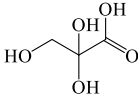
The performance comparison of photocatalytic degradation of TCH between different catalysts and the as-prepared 6BPs/CNs/BOB_{1:2}.

Catalyst	M (mg)	C (mg/L)	T (min)	V (mL)	R (%)	k (min ⁻¹)	I (mg/(g·min))	Reference
CALTCT-15	100	10	60	100	96.7	/	0.161	[2]
CT-3	50	20	150	50	92	0.016	0.123	[3]
30%In ₂ S ₃ /Bi ₂ WO ₆	100	20	120	100	96	0.024	0.160	[4]
Sol-10BP/BiOBr	100	50	90	100	85	0.021	0.472	[5]
D-TCN450	25	10	80	50	68.2	0.024	0.171	[6]
5.4%NiSe ₂ /MoS ₂	30	20	120	50	80.6	0.012	0.224	[7]
g-C ₃ N ₄ /WO ₃	40	10	180	100	79.8	/	0.111	[8]
S-TUCNov	50	10	60	50	87.7	0.032	0.146	[9]
BSO/BMO-6%	35	20	100	100	98.7	0.040	0.564	[10]
6BPs/CNs/BOB _{1:2}	50	20	60	200	88.3	0.043	1.177	This paper

Table S3

The specific information of possible degradation intermediates of TCH.

Product	Molecular formula	Retention time (min)	MS (m/z)	Supposed Structure
TC	C ₂₂ H ₂₄ N ₂ O ₈	6.66	445	
P1	C ₂₂ H ₂₄ N ₂ O ₉	/	461	
P2	C ₂₂ H ₂₄ N ₂ O ₁₀	/	477	
P3	C ₂₂ H ₂₂ N ₂ O ₉	5.50	459	
P4	C ₂₂ H ₂₈ N ₂ O ₈	5.50	449	
P5	C ₁₉ H ₁₉ NO ₅	7.13	340	
P6	C ₂₁ H ₂₅ NO ₇	/	405	
P7	C ₁₉ H ₂₀ O ₇	9.39	362	
P8	C ₂₁ H ₂₂ N ₂ O ₈	/	431	

P9	$C_{20}H_{20}N_2O_8$	6.66	417	
P10	$C_{17}H_{18}O_6$	9.39	318	
P11	$C_{15}H_{14}O_5$	9.39	274	
P12	$C_{14}H_{14}O_4$	8.42	246	
P13	$C_{14}H_{12}O_3$	5.50	227	
P14	$C_{13}H_{14}O_3$	7.48	218	
P15	$C_{11}H_{10}O$	/	158	
P16	$C_7H_{10}O_2$	/	126	
P17	$C_3H_6O_5$	/	122	

For notice, the P1, P2, P6, P8, P15, P16, and P17 were not detected in the MS spectra, which was possibly due to their extremely low concentration. Their existences have been reported in related papers, so it was feasible to analyze the possible degradation pathways using them as a reference.

Reference

- [1] Y. Yang, Z. Zeng, C. Zhang, D. Huang, G. Zeng, R. Xiao, C. Lai, C. Zhou, H. Guo, W. Xue, M. Cheng, W. Wang, J. Wang, Construction of iodine vacancy-rich BiOI/Ag@AgI Z-scheme heterojunction photocatalysts for visible-light-driven tetracycline degradation: Transformation pathways and mechanism insight, *Chemical Engineering Journal*, 349 (2018) 808-821.
- [2] B. Shao, Z. Liu, G. Zeng, Y. Liu, Q. Liang, Q. He, T. Wu, Y. Pan, J. Huang, Z. Peng, S. Luo, C. Liang, X. Liu, S. Tong, J. Liang, Synthesis of 2D/2D CoAl-LDHs/Ti₃C₂T_x Schottky-junction with enhanced interfacial charge transfer and visible-light photocatalytic performance, *Applied Catalysis B-Environmental*, 286 (2021).
- [3] Z. Zhuge, X. Liu, T. Chen, Y. Gong, C. Li, L. Niu, S. Xu, X. Xu, Z.A. Alothman, C.Q. Sun, J.G. Shapter, Y. Yamauchi, Highly efficient photocatalytic degradation of different hazardous contaminants by CaIn₂S₄-Ti₃C₂T_x Schottky heterojunction: An experimental and mechanism study, *Chemical Engineering Journal*, 421 (2021).
- [4] Z.M. He, M.S. Siddique, H.P. Yang, Y.M. Xia, J.B. Su, B. Tang, L.N. Wang, L. Kang, Z.Y. Huang, Novel Z-scheme In₂S₃/Bi₂WO₆ core-shell heterojunctions with synergistic enhanced photocatalytic degradation of tetracycline hydrochloride, *Journal of Cleaner Production*, 339 (2022).
- [5] X. Li, J. Xiong, X. Gao, J. Ma, Z. Chen, B. Kang, J. Liu, H. Li, Z. Feng, J. Huang, Novel BP/BiOBr S-scheme nano-heterojunction for enhanced visible-light photocatalytic tetracycline removal and oxygen evolution activity, *Journal of Hazardous Materials*, 387 (2020) 121690.
- [6] L. Chen, Y.X. Wang, S. Cheng, X.L. Zhao, J.Q. Zhang, Z.M. Ao, C.C. Zhao, B. Li, S.J. Wang, S.B. Wang, H.Q. Sun, Nitrogen defects/boron dopants engineered tubular carbon nitride for efficient tetracycline hydrochloride photodegradation and hydrogen

evolution, *Applied Catalysis B-Environmental*, 303 (2022).

[7] J. Jia, L.S. Zheng, K.K. Li, Y.T. Zhang, H.J. Xie, Two-electron transfer mechanism from 3D/3D nickel selenide/MoS₂ heterostructure accelerates photocatalytic hydrogen evolution and tetracycline hydrochloride removal, *Chemical Engineering Journal*, 429 (2022).

[8] H. Jing, R. Ou, H. Yu, Y. Zhao, Y. Lu, M. Huo, H. Huo, X. Wang, Engineering of g-C₃N₄ nanoparticles/WO₃ hollow microspheres photocatalyst with Z-scheme heterostructure for boosting tetracycline hydrochloride degradation, *Separation and Purification Technology*, 255 (2021).

[9] J.X. Ni, W. Wang, D.M. Liu, Q. Zhu, J.L. Jia, J.Y. Tian, Z.Y. Li, X. Wang, Z.P. Xing, Oxygen vacancy-mediated sandwich-structural TiO_{2-x}/ultrathin g-C₃N₄/TiO_{2-x} direct Z-scheme heterojunction visible-light-driven photocatalyst for efficient removal of high toxic tetracycline antibiotics, *Journal of Hazardous Materials*, 408 (2021).

[10] S.J. Li, C.C. Wang, Y.P. Liu, M.J. Cai, Y.N. Wang, H.Q. Zhang, Y. Guo, W. Zhao, Z.H. Wang, X.B. Chen, Photocatalytic degradation of tetracycline antibiotic by a novel Bi₂Sn₂O₇/Bi₂MoO₆ S-scheme heterojunction: Performance, mechanism insight and toxicity assessment, *Chemical Engineering Journal*, 429 (2022).